

Impact of the X ray edge singularity on detection of relic neutrinos in the PTOLEMY project

Zhiyang Tan (谭志阳)¹ and Vadim Cheianov^{1,*}

¹Lorentz Institute, Leiden University

(Dated: February 16, 2022)

Direct detection of relic neutrinos in a beta-decay experiment is an ambitious goal, which has for a long time been beyond the reach of available technology. One of the toughest practical difficulties that such an experiment has to overcome is that it needs to deal with a large amount of radioactive material in such a way as to not compromise the energy resolution required for the separation of useful events from the massive beta-decay background. The PTOLEMY project offers an innovative approach to this problem based on deposition of radioactive material on graphene. While such an approach is expected to resolve the main difficulty, new challenges arise from the proximity of the beta decayers to a solid state system. In this work we focus on the effect of the shakeup of the graphene electron system due to a beta-decay event. We calculate the distortion of the relic neutrino peaks as resulting from such a shakeup, analyse the impact of the distortion on the visibility of neutrino capture events and discuss what technological solutions could be used to improve the visibility of neutrino capture events.

INTRODUCTION

The discovery of the cosmic microwave background (CMB) by Penzias and Wilson [1] was a pivotal event in Big Bang cosmology. The data from WMAP (Wilkinson Microwave Anisotropy Probe), 2001 [2] and Planck in 2013 [3] gave us the snapshot of the Universe dating back to about 13 billion years ago. However, the CMB provides no direct access to the Universe within 300 000 years of the Big Bang, because electromagnetic waves could not freely propagate in that epoch. For this reason, astronomers look for an alternative messenger, a particle that had decoupled from matter earlier than the CMB. In particular, the decoupling of neutrinos is believed to have occurred just 1 second after the Big Bang. Unfortunately, the extremely weak coupling of neutrinos with matter make the detection the Cosmic Neutrino Background (CνB) a significant challenge. The principal idea of relic neutrino detection was proposed by Steven Weinberg as early as 1962 [4]. According to Weinberg, the events of capture of CνB neutrinos by beta-active nuclei should result in a weak but potentially discernible feature in the nuclei's beta spectrum. The idea was elaborated in several proposals [5, 6] centred around beta decay of Tritium, which is favored because of the relatively big product of its capture cross-section and its half lifetime [7].

Beta-decay is a type of radioactive decay in which an atomic nucleus emits a beta particle [8]. In this process, a neutron decays into a proton, and emits an electron and an anti-neutrino as well. The induced beta decay process occurs by absorbing a neutrino. The two processes are illustrated in the following two reaction equations



and

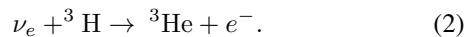


Fig. 1 depicts the theoretical beta-electron energy spectrum (called the beta-spectrum) of ${}^3\text{H}$, showing both the beta decay background and the CνB peak[9]. Since in a spontaneous

beta decay process one particle decays in three, the energy spectrum of the beta particle is continuous. In contrast, a low-energy neutrino is absorbed and only two particles are produced in a relic-neutrino induced beta decay, therefore the smoking gun signature of a relic neutrino capture is one or more discrete peaks in the spectrum, shifted about $2m_\nu$ above the beta decay endpoint. The broadening of the peaks seen in 1 reflects the finite energy resolution of the experiment, which is assumed to be close to 20 meV. The two narrow peaks in the spectrum come from the contributions of different mass eigenstates. The energy gap is only about 100 meV, so the CNB signal can only be directly probed if the energy resolution of the experiments has the same order of magnitude as the neutrino mass. However, even the most advanced to date neutrino detector, KATRIN can only achieve an energy resolution of about 1 eV [6]. Several effects may limit the energy resolution significantly of a neutrino capture experiment. For gaseous Tritium, which is used as the neutrino target in the KATRIN experiment, the most important one is the broadening of the spectrum due to the zero-point vibration of the T₂ molecular bond[6, 10].

Apart from the requirement of high energy resolution, sufficient number events is another crucial factor for the detection of CνB. The events of capture of relic neutrinos are very rare. As few as four capture events a year are expected to occur in a 100g Tritium sample [7, 11]. Moreover, even if a capture event has happened it may escape observation due to various obstructing factors. We define the effective mass of tritium as mass that contributes to the observable signal. One of the mechanisms that result in the loss of useful signal is inelastic scattering between the beta-electron and surrounding Tritium molecules. This mechanism sets a strong constraint on the effective mass of Tritium since only the electrons emitted within the mean free path of the sample boundary contribute to the signal and the rest of electrons are lost to the background [12, 13].

Taking into account the limitations imposed by both the vibrations of the T₂ bond and the losses to inelastic scattering one can estimate the working volume of gaseous Tritium

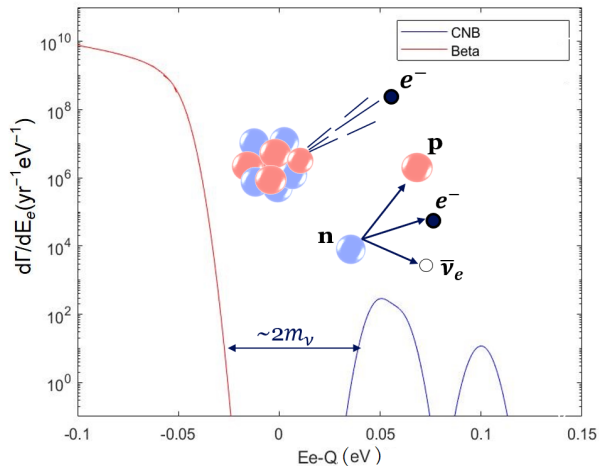


FIG. 1: Beta decay spectrum and the sketch of the beta decay process. The blue curve depicts the CNB spectrum, and the red curve represents the beta decay spectrum, and they are separated by an energy gap, which has an order of magnitude twice the neutrino mass ($2m_\nu$). The annotation of the horizontal axis is the kinetic energy of the emitted electron measured from the endpoint of the beta decay spectrum, and the annotation of the vertical axis is the events observed at a certain energy per year. The area behind each curve represents the events per year, and the area behind the CNB curve is only 4.

required for a $C\nu B$ detection experiment. Firstly, we note that only about 0.013 percent of the beta-decay events occur without excitation of the vibrational levels of the He^+T complex [14], that is without the loss of an emitted electron to the spontaneous decay background. This implies that in the ideal case of no losses due to collisions of an electron with other molecules, about 800kg of molecular Tritium will be required to achieve four counts per year. The requirement that the sample size be less than the inelastic mean free path of an electron imposes the lower bound on the working volume $V > (N_{\text{eff}}\sigma_{e-\text{T}})^{3/2}$ [15], where N_{eff} is the number of atoms in the sample and $\sigma_{e-\text{T}}$ is the scattering cross-section. For a 800kg sample the resulting minimal volume is $\sim 10^{10} \text{ m}^3$, which is by all counts impracticable.

In order to get rid of the molecular vibrations and to contain the required amount of radioactive material within small enough volume, the PTOLEMY collaboration [16, 17] proposed to deposit Tritium atoms on graphene. In such a design, beta electrons emitted into the vacuum surrounding a decorated graphene sheet are electromagnetically guided into the calorimeter without experiencing significant collisional losses. Due to graphene being an electric conductor, all beta-emitters can be maintained at the same electrostatic potential thus avoiding inhomogeneous broadening of the beta spectrum. Assuming that the surface coverage of graphene by Tritium approaches the fully tritiated limit of $3 \times 10^{19} \text{ m}^{-2}$

[11, 18] and a possibility to arrange graphene planes into a vertical stack, with 1 mm separation between the layers [19], 100 grams of Tritium could be contained within the 10^3 m^3 volume, which is a seven orders of magnitude improvement compared to the gas phase experiment.

While the emitter-on-solid design seems to resolve the working volume problem, it creates a host of other complications arising from the interaction of the beta-emitter with the substrate. Firstly, by virtue of Heisenberg's uncertainty principle the very fact of spatial confinement of a radioactive nucleus results in an uncertainty in nucleus's velocity, which propagates to an error in the detected kinetic energy of the beta-electron. For Tritium the effect is big enough to make it practically impossible to separate neutrino capture events from the beta decay background [20]. This problem could likely be resolved by abandoning Tritium in favour of heavy radioactive isotopes such as ^{171}Tm or ^{151}Sm [21]. Heisenberg uncertainty, however, is not the only issue arising from the proximity of the beta-emitter to a solid state system. A number of other potentially detrimental effects is listed in Ref. [20] and discussed in more detail in Ref. [22]. In particular, Ref. [22] identifies the shakeup of the electron system in graphene due to the sudden formation of a charged He^+ ion as a possible source of significant, up to 15 eV, broadening of the neutrino capture line in the beta-spectrum, which if true would be prohibitively large for the experiment.

In this work, we investigate the effect of the shakeup of the Fermi sea in graphene on the line shape of an emitted beta-electron. We exploit the straightforward mapping of the problem on the classic X-ray edge singularity problem. It is well known that the X-ray absorption spectra (XAS) and emission spectra (XES) of metals have a power-law singularity near the emission threshold, which is called X-ray edge singularity. The theory of X-ray edge singularity was proposed by Mahan [23], and elaborated in the works by Nozères, and De Dominicis [24–26], and Schotte and Schotte [27]. These works linked the Fermi-edge singularity to the shakeup of the Fermi sea due to the hole left behind after the X-ray emission. The peculiar power-law shape of the X-ray edge was found to arise from the Anderson orthogonality catastrophe (AOC) [28].

The classical X-ray edge problem occurs in normal metals. Our case has two peculiarities. Firstly, we need to investigate the X-ray edge singularity in graphene, which unlike a typical metal is two-dimensional and has a Dirac-like excitation spectrum. Secondly, we need to understand the details of the X-ray edge down to the neutrino mass scale, which is on the order of 10 meV. Such a resolution is at the limit of modern X-ray optics therefore the theory of X-ray edge singularity does not typically look into the details of the line shape within such a narrow window. In this work we will apply the theory of X-ray edge singularity to a beta decay process on graphene taking into account effects that influence the line shape on all scales relevant to the PTOLEMY experiment.

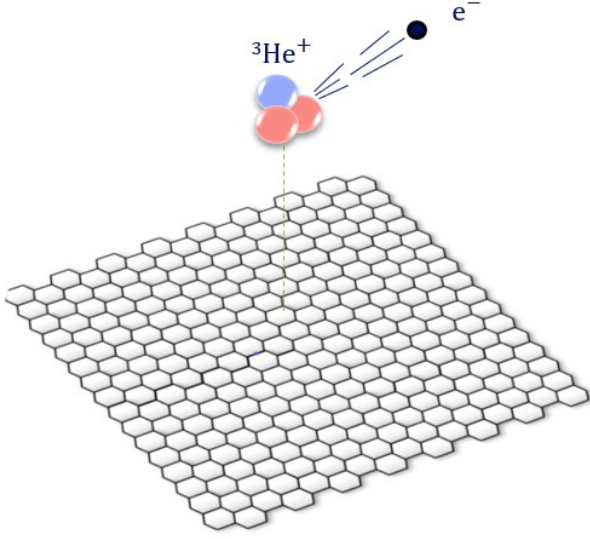


FIG. 2: Sketch of the beta emitter and graphene sheet. ${}^3\text{He}^+$ is the production of tritium beta decay, and it introduces a sudden localized perturbation in the electron system of graphene. This sudden localized perturbation causes an X-ray edge, which changes the beta decay spectrum.

FORMULATION OF THE PROBLEM

In this section, we formulate the mathematical model of beta-emission on graphene. This section is structured as follows, firstly, we give the physical description of the problem; then we list our main assumptions; then, we explain the approximation scheme used for the calculation of the observed emission line. Everywhere in the text we refer to the beta-emitter as Tritium, although the model and the results apply without change to any radioactive isotope.

We consider a Tritium atom attached to a graphene sheet either by the Van der Waals force or through the formation of a covalent bond with a carbon atom. After capturing an incoming neutrino, the Tritium atom converts into a Helium ion, releasing a fast outgoing electron as depicted in Fig(2). The sudden emergence of a positively charged Helium ion next to the graphene sheet triggers local rearrangement the material's electronic structure, in the exact same manner as a core hole in an X-ray emission experiment does. In the latter case, such a rearrangement is known to result in the X-ray edge singularity in the emission spectrum, which is seen as broadening of the emission line into an asymmetric shape having a power-law singularity at the emission edge. We expect to see a similar phenomenon in the β -spectrum of Tritium on graphene.

To analyse the problem, we make the following assumptions:

(1) The recoil effect between the outgoing electron and the helium ion on the X-ray singularity can be neglected. The typical recoil energy of the Helium ion is about 3.38 eV, which has the same order of magnitude the Fermi energy in graphene,

however the mass of the Helium ion is about 6000 times the mass of an electron, therefore we are safe to say that the Helium ion remains static throughout the emission process.

(2) We neglect the electron-electron scattering in the graphene sheet. We include the Coulomb interaction between electrons only in the form of the RPA corrections to the dielectric response of graphene.

(3) We only focus on the processes which do not result in the excitation of internal degrees of freedom of the Helium ion. Only such processes are relevant to the neutrino capture experiment.

(4) We assume that the graphene sample spatially uniform. Where we analyse the effect of disorder, we assume that the disorder is spatially uniform.

(5) We assume the lateral position of the Helium ion relative to the graphene sheet is insignificant. This is because the X-ray edge singularity is an infrared phenomenon, arising from the long-range Coulomb interaction, which is insensitive to the exact position of the Coulomb centre inside the unit cell.

(6) We neglect the scattering potential induced in graphene by neutral Tritium as compared with the long-range Coulomb potential resulting from the He^+ ion.

Based on these assumptions, we formulate the Hamiltonian

$$H = H_0 + H_I + H_{h-g} \quad (3)$$

which comprises the kinetic part, interaction part and the coupling between the helium ion and graphene. The kinetic part is trivial, and it is the sum of the kinetic energies of all particles involved in the process

$$\begin{aligned} H_0 = & m_\nu c^2 \int \nu^\dagger \nu d^3x + m_h c^2 \int h^\dagger h d^3x \\ & + m_t c^2 \int t^\dagger t d^3x + \sum_k e_k^\dagger e_k \left(\frac{\hbar^2 k^2}{2m_e} + m_e c^2 \right) \\ & + \sum_s \sum_k s \hbar v_F k C_{k_s}^\dagger C_{k's}. \end{aligned} \quad (4)$$

Here m_ν is the mass of a neutrino, m_h is the mass of helium ion, and m_t is the mass of the tritium atom. The ionization energy of the helium atom is insignificant compared to the emission energy of beta decay so that we can ignore the energy difference between the helium ion and helium atom. ν^\dagger is the creation operator for the neutrino, h^\dagger is the creation operator for helium ion, t^\dagger is the creation operator for the tritium ion, e_k^\dagger is the creation operator for the outgoing electron, v_F is the Fermi velocity, $C_{k_s}^\dagger$ and $C_{k's}$ are the creation and annihilation operators for the electrons in the graphene respectively, and s is the band index of the graphene. The spin and valley indices have been absorbed into the band index.

The term

$$H_I = \int G_F \nu t h^\dagger e^\dagger d^3x, \quad (5)$$

is the effective Hamiltonian of the beta-decay process, where G_F is the effective beta decay interaction constant absorbing

the details of ultrafast electroweak processes inside the nucleus [8, 29],

The final term in the Hamiltonian, H_{h-g} describes the interaction between the electrons in graphene and the charged Helium ion, which suddenly emerges due to the beta-decay process. We write this term as follows:

$$H_{h-g} = - \int \rho(x) V(x) h_0^\dagger h_0 d^2x. \quad (6)$$

Here $h_0^\dagger h_0$ is the Helium ion counting operator,

$$V(x) = \frac{e^2}{4\pi\epsilon\epsilon_0\sqrt{d^2 + x^2}} \quad (7)$$

is the Coulomb potential of the ion in the graphene plane, and

$$\rho(x) =: \psi^\dagger(x)\psi(x) :, \quad (8)$$

is the two-dimensional density of electrons in graphene. We have denoted the dielectric constant of the graphene as ϵ and the distance between the helium ion and the graphene as d . The field operator of an electron in graphene $\psi(x)$ admits for the standard plane wave decomposition

$$\psi(x) = \sum_{k,s} C_{ks} \psi_{ks} e^{-i\vec{k}\cdot\vec{x}} \quad (9)$$

where ψ_{ks} is the spinor of the dirac electrons in the graphene,

$$\psi_{ks} = \frac{1}{\sqrt{2}} \begin{pmatrix} e^{-i\theta_k} \\ s \end{pmatrix} \quad (10)$$

with $\theta_k = \arctan(k_y/k_x)$.

In the standard vein of beta decay theory, the transition probability is given by Fermi's golden rule

$$W = \frac{2\pi}{\hbar} \sum_f \left| \langle 0|_t \langle 0|_\nu \langle k|_e \langle 1|_h \langle \lambda| \int G_F \nu d h^\dagger e^\dagger d^3x \right. \\ \left. |1\rangle_t |1\rangle_\nu |0\rangle_e |0\rangle_h |FS\rangle \right|^2 \delta(E_f - E_i) \quad (11)$$

where $|\lambda\rangle$ is the final state of the graphene with the energy E_λ and $|FS\rangle$ is the Fermi sea of the graphene with energy E_0 . The total energy of final state in the process is $m_e c^2 + \frac{\hbar^2 k^2}{2m_e} + E_\lambda + m_h c^2$, and the energy of initial state is $m_\nu c^2 + m_t c^2 + E_0$. The final state is the tensor product of the neutrino state, the outgoing electron state, and the graphene electron state. We can sum over the normal beta decay part and graphene part independently. We use index f' to denote the final state of beta decay and use index λ to denote the final state of electrons in graphene. Moreover, we can express the total transition probability as a convolution of the transition probability function of beta decay and graphene spectral

density function. Hence, the expression of the total transition probability can be simplified to

$$W = \frac{2\pi}{\hbar} \int dE \sum_{f'} \sum_{\lambda} |V_{if'}|^2 |\langle \lambda|FS\rangle|^2 \delta(E + E_\lambda - E_0) \\ \times \delta(E_k - Q - E) \\ = (\Gamma * A)(E_k), \quad (12)$$

where $Q = m_t c^2 + m_\nu c^2 - m_e c^2 - m_h c^2$ is the emission energy of beta decay (equal to 18.6 KeV, for Tritium), E_k is the kinetic energy of the beta electron, $\Gamma(E)$ is the beta decay transition rate of a single atom in vacuum, and $A(E)$ is the electron spectral density function in graphene. Following the convention, we can consider dW/dE_k as observable beta decay rate at given electron kinetic energy corrected by the electron shakeup process

$$\frac{d\tilde{\Gamma}}{dE_k} = \frac{dW}{dE_k} = \left(\frac{d\Gamma}{dE_k} * A \right) (E_k), \quad (13)$$

where $\tilde{\Gamma}$ pertains to the observed electron emission spectrum as opposed to the hypothetical emission spectrum of a single atom in vacuum. The discussion above also valid for the process of background neutron decay. We have found out that the smeared beta decay spectrum is nothing but the convolution between the spectral density function of graphene and the original beta decay spectrum. This result is vital to us since it tells us the influence of the X-ray edge in the PTOLEMY project. Later, we will show that the spectral density function does have an X-ray edge.

LINKED CLUSTER EXPANSION

In this section we assume that Helium ion is screened instantaneously. This assumption does not work well in graphene and we will revise it later, however at this stage we would like to keep our discussion as simple as possible focusing on the key physics of the problem. With the help of the random phase approximation and neglecting time retardation, we obtain the effective static dielectric constant of graphene

$$\epsilon = \frac{1 + \kappa}{2} + \frac{2\pi e^2}{q} \frac{g_s g_v q}{16\hbar v_F} \quad (14)$$

where κ is the external dielectric constant of the substrate, the degeneracy factor $g_s = 2$, $g_v = 2$, and $v_F \approx 10^6$ m/s. If the graphene is suspended in vacuum, then $\epsilon \approx 4.4$.

The spectral density function $A(E)$ is the central object of interest, so we will investigate its property further in this section. The expression for it is

$$A(E) = \sum_{\lambda} |\langle \lambda|FS\rangle|^2 \delta(E + E_\lambda - E_0) \\ = \frac{1}{2\pi\hbar} \int dt \langle FS| e^{-iH_\lambda t/\hbar} |FS\rangle e^{iE_0 t/\hbar} e^{-iEt/\hbar}, \quad (15)$$

where H_λ is the Hamiltonian of the graphene after the beta decay. We can express it in momentum space,

$$H_\lambda = \sum_s \sum_k s\hbar v_F k C_{ks}^\dagger C_{k's} - \frac{1}{L^2} \sum_{ss'} \sum_{kk'} V(k, k') F_{ss'}(k, k') C_{ks}^\dagger C_{k's'} \quad (16)$$

with

$$F_{ss'}(k, k') = \frac{1}{2} [ss' + \exp(i\theta_k - i\theta_{k'})] \quad (17)$$

and

$$V(k, k') = \frac{2\pi e^2 \exp(-|k' - k|d)}{\epsilon |k - k'|} \quad (18)$$

To calculate the spectral density function $A(E)$, we first focus on the density function, which is its Fourier transform

$$\rho(t) = \langle \text{FS} \left| e^{-iH_\lambda t/\hbar} \right| \text{FS} \rangle e^{iE_0 t/\hbar}. \quad (19)$$

One can recognize $-i\Theta(t)\rho(t)$ as the core hole Green function in the conventional X-ray singularity problem [24, 25, 30–32]. Using linked cluster expansion method [32–34], we can express the density function $\rho(t)$ in another way.

$$\rho(t) = \exp \left[\sum_l F_l(t) \right] \quad (20)$$

where $F_l(t)$ is the l -th connected diagrams,

$$F_l(t) = \frac{(-i)^l}{l} \int_0^t dt_1 \cdots \int_0^t dt_l \langle TV(t_1) \cdots V(t_l) \rangle_{\text{connected}}. \quad (21)$$

$V(t)$ is the interaction term in the Dirac picture. The first term is just the self-energy term E_i , so it can be absorbed into the threshold energy. Assuming the interaction is weak, we can restrict ourselves to the second term [32].

$$F_2(t) = - \int_0^\infty \frac{du}{u^2} R_e(u) (1 - e^{-iut}) \quad (22)$$

where

$$R_e(u) = \frac{1}{\pi L^2} \sum_q |V(q)|^2 \Lambda(q, u) \quad (23)$$

and

$$\Lambda(q, u) = \text{Im} P^{(1)}(q, u). \quad (24)$$

where $P^{(1)}(q, u)$ is the polarizability function. The expression of the polarizability is given in many references [32, 35], so we just quote the result

$$P^{(1)}(q, u) = \frac{-ig'}{L^2} \int_{-\infty}^\infty \frac{dE}{2\pi} \sum_{p,s,s'} |F_{ss'}(p, p+q)|^2 \times G_{ss}(p, E) G_{s's'}(p+q, E+u), \quad (25)$$

where $G_{ss}(P, E)$ is the Green function for graphene, g' is the degeneracy, and it is 4 for intrinsic graphene. The polarizability function of the intrinsic graphene was calculated in the references [36–38]. In particular, its imaginary part gives

$$\Lambda(q, u) = \frac{q^2}{4\sqrt{u^2 - v_F^2 q^2}} \Theta(u - v_F q). \quad (26)$$

To calculate $R_e(u)$, one needs to substitute eq. (26) into eq. (23). To simplify the calculation, we omit the exponential factor in the eq. (18), and the potential becomes

$$V(k, k') = \frac{2\pi e^2}{\epsilon |k - k'|} \quad (27)$$

Although this crude simplification is only valid near the edge of the spectral density function, it gives us a physics insight in the first step. Later, we will recover the effect of the distance d in the next section. Then we have

$$R_e(u) = gu, \quad (28)$$

where

$$g = \frac{e^4}{2\epsilon^2 v_F^2} \quad (29)$$

Using the effective dielectric constant we get in the previous step, we can find $g \approx 0.125$. Substituting it into the expression of F_2 , thus one can get

$$F_2(t) = -g \int_0^{\xi_0} \frac{(1 - e^{-iut}) du}{u} \approx -g \int_{1/it}^{\xi_0} \frac{du}{u} \approx -g \ln(1 + it\xi_0) \quad (30)$$

Note that due to the logarithmic divergence of the integral we had to use an arbitrary ultraviolet cutoff ξ_0 to complete the calculation. This cutoff parameter is important for the estimate of the visibility of the C ν B peak, therefore it cannot be chosen arbitrarily. The physical meaning and the value of ξ_0 will be clarified later.

The expression (30) is valid only for large enough t , that is $\xi_0 t \gg 1$. The expression for the density function is obtained from eq. (30),

$$\rho(t) = \exp(-iE_i t - g \ln(1 + it\xi_0)). \quad (31)$$

SPECTRAL DENSITY FUNCTION

In this section, we give an explicit formula of the spectral density function of graphene. Furthermore, we investigate the influence of the height from the Helium ion above the graphene sheet, as well as the influence of disorder and the dynamical screening on the spectral density function.

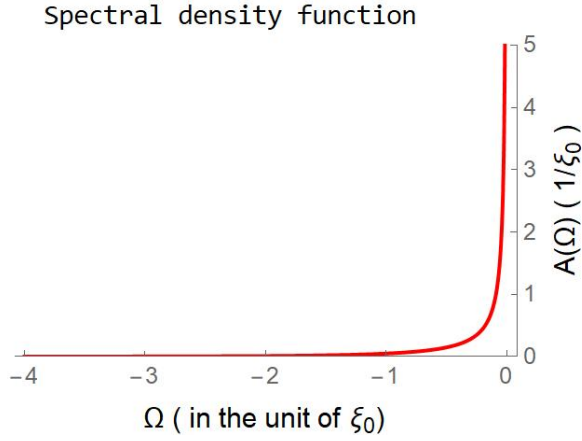


FIG. 3: The spectral density function of graphene at a given energy. $A(\Omega)$ describes the possibility of graphene absorbing the outgoing electron's energy. The energy is measured in the unit of cut-off energy ξ_0 .

The Fourier transform of eq. (31) gives the spectral density function of graphene at the given energy, and it is exactly the gamma distribution function.

$$\begin{aligned} A(\Omega) &= \int_{-\infty}^{\infty} \frac{dt}{2\pi} e^{-iEt} \rho(t) \\ &= \Theta(-\Omega) \frac{\exp(\Omega)}{\xi_0 \Gamma(g) (-\Omega)^{(1-g)}} \end{aligned} \quad (32)$$

with

$$\Omega = (E + E_i)/\xi_0 \quad (33)$$

The spectral density function obeys the gamma distribution, and the result coincides with that for a metal with a local constant interaction [32–34]. The gamma distribution function has two parameters: one is the shape parameter, which is the coupling constant in our problem, and another one is the scale parameter, which has so far remained an arbitrary cut-off parameter. The coupling constant determines how sharp the peak is near the edge, and the cutoff energy determines how many events are lost in the long tail of the spectral density function. Fig. 3 represents the spectral density function. As we can see in Fig. 3, the function sharply diverges when Ω goes to zero. In other words, the differential emission rate is the largest when no electron excitations are created in graphene at the end of the process.

Influence of the Height

In the previous discussion, we have calculated the spectral density function and obtained its shape parameter g . However, the cutoff energy remains unknown. Typically, one would expect the cutoff energy to be associated with the electron bandwidth or the Fermi energy. In this section we find that

the cutoff energy is dictated by the height of helium ion above the graphene sheet. Indeed, for any given d the expression of $R_e(u)$ is

$$\begin{aligned} R_e(u) &= e^4 \int_0^{u/v_F} \frac{qe^{-2qd} dq}{2\epsilon^2 \sqrt{u^2 - v_F^2 q^2}} \\ &= gu + \frac{\pi gu}{2} \left[L_1 \left(\frac{2du}{v_F} \right) - I_1 \left(\frac{2du}{v_F} \right) \right] \end{aligned} \quad (34)$$

where $L_1 \left(\frac{2du}{v_F} \right)$ and $I_1 \left(\frac{2du}{v_F} \right)$ are modified Struve function and modified Bessel function, respectively.

This equation may look slightly intimidating however its intuitive meaning is simple. The X-ray edge singularity is an infrared phenomenon, so only long distance interaction is significant for it. Thus we can eliminate the short-distance structure of the Coulomb interaction. If $q \ll 1/(2d)$, the Yukawa type potential in eq. (34) recovers to the normal Coulomb potential, thus giving a natural cutoff energy $\xi = \hbar v_F/2d$. From asymptotic analysis (details are in App: A1), we find that the spectral density function was the same form as in Eq. (32) albeit with a cutoff energy ξ' ,

$$\xi' = \frac{\xi_0}{1 + 2d\xi_0/v_F}. \quad (35)$$

ξ_0 is a microscopic parameter on the order of the bandwidth energy. Assuming that $\xi_0 \ll v_F/d$, which is particularly accurate in case of rare earth atoms deposited on graphene, one finds

$$\xi = \lim_{\xi_0 \rightarrow \infty} \xi' = \frac{\hbar v_F}{2d} \quad (36)$$

The expression (36) should replace ξ_0 as the scale factor in the line shape equation Eq. (32). One can see that the scale factor depends on the height d , so one could potentially manipulate the line shape by adjusting the height of the ion.

Influence of disorder

Until now, we have only considered intrinsic graphene, uncontaminated and ungated. However, a finite density of beta emitters in graphene inevitably introduces disorder, which changes the mean free path and the density-density response function of electrons. Intuitively, one should expect that if the time scale associated with the inverse energy resolution of the beta detector is greater than the mean free time in graphene, i.e., $\tau_{\text{res}} \gg \tau$, then one needs to take into consideration the effect of electron diffusion on the polarizability function and thus the coupling constant. Luckily, as we will show momentarily, if the concentration of tritium is lower than the $5 \times 10^{11}/\text{cm}^2$, then the effect of disorder is negligible.

We consider eq. (15), in the presence of many random impurities, focusing on the impurity-average effect. The impurity-average polarizability function $P_{\text{imp}}(q, \omega)$ is [35, 39,

40]

$$P_{\text{imp}}(q, \omega) = \frac{P^{(1)}(q, \omega + \frac{i}{\tau})}{1 + (1 - i\omega\tau)^{-1} \left[\frac{P^{(1)}(q, \omega + \frac{i}{\tau})}{P^{(1)}(q, 0)} - 1 \right]} \quad (37)$$

where τ is interpreted as momentum relaxation time or the quasiparticle lifetime. The required energy resolution of the detector is ω_{res} is about 10 meV, therefore the resolution time τ_{res} is $\sim 10^{-13}$ s. If $\omega_{\text{res}} \gg 1/\tau$, we can neglect the effect of impurities, and the polarizability function recovers to the Lindhard function [39]. Otherwise, we need to consider both diffusive and ballistic regimes.

Apart from impurities, phonons can also influence the mean free time of graphene. However, one can keep the system in a very low temperature to reduce the phonon scattering. For intrinsic graphene under liquid nitrogen temperature, the momentum relaxation time is about one ps [41, 42], which is one order greater than the resolution time. Therefore, we can treat electrons of the graphene ballistically within the resolution time. However, the physisorption or chemisorption of tritium atoms on the graphene changes the mean free time of electrons. Electrons in the graphene are not so dense as them in metals, so that impurities have significant effects on the transport properties of graphene. For physisorption, the binding energy of the tritium atom is about 0.2 eV, so the potential difference between the tritium atom and carbon sheet is about 0.2 eV [43–45]. Since the energy of an electron is about 1 eV, most electrons change their momentum slightly. Therefore, we do not need to consider the impurity effects in the physisorption case.

However, it is very tricky for chemisorption since the binding energy has the same order of magnitude as the electrons' energy [45, 46]. For pure graphene, the hybridization of its electronic orbital is sp^2 , contributing a π electron. For tritiated graphene, the chemical bonding between a tritium atom and a carbon atom changes the hybridization from sp^2 to sp^3 . The π orbital is tightly bounded for the sp^3 hybridization, so the tritium atom effectively acts as a vacancy. Thus, we can use the midgap model to characterize the potential induced by the tritium atoms [43, 47, 48]. The potential is profiled as

$$U(r) = \begin{cases} \infty, & \text{if } 0 < r \leq R' \\ U_0, & \text{if } R' < r \leq R \\ 0, & \text{if } r > R, \end{cases} \quad (38)$$

where R' is the radius of a hydrogen atom, and R is the radius of a carbon atom. The mean free time is defined from the following expression

$$\frac{\hbar}{\tau_k} = \frac{8n_i}{\pi\rho(E_k)} \sin^2 \delta(k), \quad (39)$$

where $\delta(k)$ is the phase shift of electrons with momentum k , and $\rho(E_k)$ is the density of state, with the explicit form

$$\rho(E_k) = \frac{2E_k}{\pi\hbar^2v_F^2}. \quad (40)$$

Using the method in the paper [48], we can obtain the phase shift at $k \approx 0$,

$$\delta(k) = -\frac{\pi}{2} \frac{1}{\ln(2kR')}. \quad (41)$$

We expand the sine function in eq. (39) for $kR' \ll 1$. Thus it gives the mean free time

$$\begin{aligned} \tau_k &= \frac{\hbar\rho(E_k)}{2\pi n_i} (\ln kR')^2 \\ &= \frac{k}{\pi^2 v_F n_i} (\ln kR')^2, \end{aligned} \quad (42)$$

where n_i is the impurity concentration. The mean free path has a minimal value at $kR' = e^{-2}$, and its minimum value is

$$\tau_{\text{min}} = \frac{4e^{-2}}{\pi^2 v_F n_i R'} \quad (43)$$

If τ_{min} is much greater than the resolution time, we can neglect the impurity effect. It means that

$$\frac{4e^{-2}}{\pi^2 v_F n_i R'} \gg 1/\omega \sim 10^{-13} \text{ s} \quad (44)$$

R' is about 1 Å, so we find the condition for a maximum impurity concentration.

$$n_i \ll \frac{4e^{-2}\omega}{\pi^2 v_F R'} = 5 \times 10^{11} / \text{cm}^2 \quad (45)$$

The above discussions are also valid for other onsite impurities, but the safe concentrations of different beta emitters are different. In conclusion, if the concentration of tritium atoms is less than $5 \times 10^{11} / \text{cm}^2$, then one should expect the effect of the disorder to be negligible.

Influence of Dynamic Screening

The instantaneous screening assumption is not valid in the tail of the spectral function of graphene. While, if the weight of the tail is too high, it will cause the beta decay spectrum to broaden widely, and it may take many years to observe a single event. To get a more rigorous result, we need to consider the dynamic screening effect. The dynamic screening potential is

$$V(q, \omega) = \frac{V_i(q, \omega)}{\epsilon(q, \omega)} \quad (46)$$

For a sudden external potential [49],

$$V_i(q, \omega) = \frac{V(q)i}{\omega + i\delta}. \quad (47)$$

δ is an infinitesimal quantity, and $V(q) = 2\pi e^2 / (\kappa q)$ is the bare Coulomb potential. We notice that $\epsilon^{-1}(q, \omega) - 1$ is the

susceptibility function so we can use the Kramers-Kronig relations.

$$\frac{1}{\epsilon(q, \omega)} - 1 = -\frac{1}{\pi} \int_{-\infty}^{\infty} d\omega' \text{Im} \left(\frac{1}{\epsilon(q, \omega')} - 1 \right) \frac{1}{\omega - \omega' + i\delta} \quad (48)$$

Substituting it into the expression of dynamic screening potential and performing the Fourier transform, one can find the time-dependent screening potential.

$$\begin{aligned} V(q, t) &= \int_{-\infty}^{\infty} V(q, \omega) e^{-i\omega t} d\omega \\ &= \frac{V(q)\theta(t)}{\pi} \int_{-\infty}^{\infty} \frac{1 - e^{-i\omega' t}}{\omega'} \text{Im} \left(\frac{1}{\epsilon(q, \omega')} - 1 \right) d\omega' \\ &\quad + V(q)\theta(t) \end{aligned} \quad (49)$$

In the large time limit, the oscillating term disappears, so the potential becomes

$$V(q, \infty) = \frac{V(q)}{\epsilon(q, 0)} \quad (50)$$

For graphene, $\epsilon(q, 0)$ does not depend on q , so that we can denote $\epsilon(q, 0)$ as ϵ . The first term in the last line vanishes in the short time limit, so the potential turns into the bare potential.

$$V(q, 0) = V(q) \quad (51)$$

For an arbitrary time, we can express $V(q, t)$ as

$$\begin{aligned} V(q, t) &= \frac{V(q)\theta(t)}{\epsilon(q, 0)} - \frac{V(q)\theta(t)}{\pi} \int_{-\infty}^{\infty} d\omega' \frac{e^{-i\omega' t}}{\omega'} \\ &\quad \times \text{Im} \left(\frac{1}{\epsilon(q, \omega')} - 1 \right) \end{aligned} \quad (52)$$

From detailed analysis (see [App: A2](#)), we found out that the spectral density function is the same as the previous result in eq. (32), but with a different coupling constant

$$g_1 = g + \int_1^{\infty} \frac{2g\epsilon a \log(\omega + \sqrt{\omega^2 - 1})}{\pi \omega^2 (\omega^2 - 1 + a^2)} d\omega, \quad (53)$$

where $\xi_0 = \frac{\hbar v_F}{2d}$.

If graphene is suspended in vacuum, then $g = 0.125$, and $g_1 \approx 0.200$. For graphene on SiO_2 , the coupling constant g is about 0.065, and $g_1 \approx 0.090$. As one can see in Fig. 4, the dynamic screening effects of intrinsic graphene significantly change the coupling constant at a small dielectric constant, and this can be understood intuitively. For intrinsic graphene, the Fermi energy is zero, therefore there is no intrinsic time scale. For long wave-length scattering, the screening time is about $1/(v_F q)$, which is also the time scale for the Fermi sea shakeup effect at the energy scale $v_F q$, so we cannot separate the screening of the Coulomb potential from the formation of the X-ray edge singularity. Hence, the dynamical screening effects have a considerable influence on the coupling constant.

In contrast, the Fermi energy is non-zero for normal metals and gated or doped graphene, so the static screening is a good approximation near the edge in those cases. In the large dielectric constant limit, one can see from Fig. 4(b), the ratio of the dynamic coupling constant and static coupling constant approaches 1. It can be understood from eq. (14) and eq. (53), when the external dielectric constant is big enough, it makes the dominant contribution to the total dielectric constant.

To summarize, the dynamical screening effect has a considerable influence on the coupling constant in intrinsic graphene, but it can be suppressed by applying an external gate voltage or increasing the dielectric constant of the substrate.

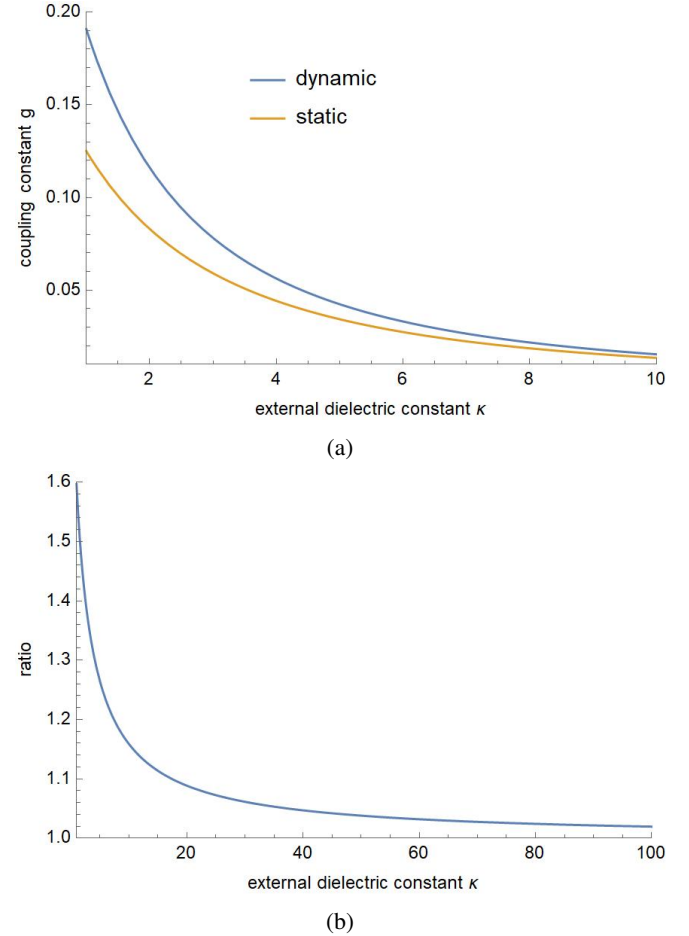


FIG. 4: Fig. 4(a) depicts the coupling constant with different external dielectric constants. κ describes the dielectric constant of the substrate, and g is the graphene's coupling constant. The blue curve represents the coupling constant considering the dynamic screening effect, and the orange curve representing the coupling constant in the static screening approximation. Fig. 4(b) describes the ratio of the dynamic coupling constant and the static coupling constant. In the large dielectric constant limit, the ratio approaches 1.

Influence of the helium ion's lifetime

In the previous discussion, we assumed that the lifetime of the Helium ion is infinite, however in reality this is not true. A positively charged ion is generally unstable and tends to capture an electron from its chemical environment. In the traditional X-ray edge singularity context such capture processes usually occur through the Auger effect. The life time of an ion formed after the beta decay process is unknown, it depends on many environmental circumstances and should probably be a matter for experiment to determine. Here, we do not attempt to estimate it. Rather we investigate how the finite life time of the Helium ion influences the visibility of the $C\nu B$ signal.

Semi-empirically, one can contain the influence of the helium ion's lifetime by calculating the convolution of the spectral density function and a Lorentzian distribution function [32].

$$A'(E) = \int_{-\infty}^{\infty} A(\mathcal{E})L(E - \mathcal{E})d\mathcal{E} \quad (54)$$

where $A(\mathcal{E})$ is graphene's spectral density function that we obtained before and $L(E)$ is the Lorentzian distribution function,

$$L(E) = \frac{\Gamma/2}{\pi[E^2 + (\Gamma/2)^2]}. \quad (55)$$

$\tau = \hbar/\Gamma$ is the lifetime of the helium ion. Inserting eq. (55) into eq. (54), then one found the convolved spectral density function is

$$A'(\Omega_1) = \begin{cases} \text{Im} \left[\frac{e^{\Omega_1} \Gamma(1-g, \Omega_1)}{\pi \xi_0 \Omega_1^{1-g}} \right], & \Gamma \neq 0 \\ A(\Omega), & \Gamma = 0 \end{cases} \quad (56)$$

where $\Omega_1 = (E - i\Gamma/2)/\xi_0$. To get an intuitive understanding, we plotted a figure of $A'(\Omega_1)$ when $g = 0.125$, $\xi_0 = 1$ eV, and $\Gamma = 0.2$ eV, as shown in Fig. 5. Generally, the effect of a finite life time is negligible if Γ is much less than the energy resolution of the electron detector. However, if Γ exceeds ω_{res} it may easily become the next experimental bottleneck.

DISCUSSION

In this section, we show how the results of the previous sections translate into the visibility of the $C\nu B$ signal in the PTOLEMY experiment. From eq. (13), we know that we can get the correct beta decay spectrum by performing a convolution between the spectral density function and the beta decay spectrum in vacuum. Using Mathematica, we plotted the beta decay spectrum with, $m_{\text{lightest}} = 50$ meV. As can be seen from comparison of Fig. 6(a) and Fig. 6(b), each cosmic neutrino background peak will be broadened into an asymmetric line having a sharp maximum near the actual neutrino mass and a long power-law tale stretching into the beta decay background. Using the calculated spectrum, we can obtain the

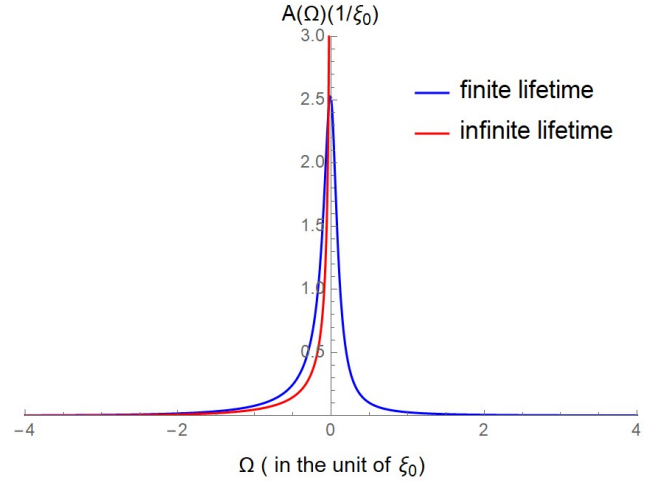


FIG. 5: The spectral density function taking into account the influence of the finite lifetime of the Helium ion (blue curve) is compared with the spectral density function at infinite life time (red curve). As one can see, at finite life time the the sharp Gamma distribution is broadened into a smooth asymmetric peak. In this plot we take $g = 0.125$, $\xi_0 = 1$ eV and $\Gamma = 0.2$ eV.

visibility, that is the number of events in the non-overlapping region in the spectrum. For the calculation of visibility we assume the amount of radioactive material equivalent to four capture events per year (about 100 g in the case of Tritium).

Based on the previous results, we know that the visibility depends on four parameters, lightest mass of the neutrino, the coupling constant, the distance from the helium ion to the graphene sheet, and the lifetime of the helium ion. We evaluate the PTOLEMY project's sensitivity to those parameters by making the plots of the visibility in different parameter planes. In Fig. 7 we show the dependence of the visibility on the lightest mass of neutrino and the coupling constant. As shown in Fig. 7, the smaller the coupling constant and the larger lightest mass of the neutrino, the better the visibility that the PTOLEMY project has. This result can be explained by the fact that a large coupling constant leads to a sharper distribution, which causes the beta decay spectrum less broadening.

Another parameter that has a big influence on the visibility of the PTOLEMY project is the lifetime of the helium ion. In Fig. 8 one can see that PTOLEMY project's visibility is very low when the Helium ion's lifetime is smaller than 1 fs. However, one can still achieve the PTOLEMY project's visibility beyond three if the helium ion's lifetime is greater than 10 fs.

Apart from the those three parameters, the distance from the ion to graphene affects the cutoff energy and therefore also influences the visibility of the PTOLEMY project. Smaller cutoff energy means less weight in the long tail of the gamma distribution, therefore fewer losses and better visibility. Indeed, as one can see from Fig. 9, visibility increases with the helium ion's height. Note that compared with the previous three parameters the influence of height on visibility is less

pronounced, at least for a small enough coupling constant. This is explained by the fact that for small g a lot of spectral weight is concentrated in the infrared region near the X-ray edge therefore the visibility is less sensitive to the ultraviolet cutoff.

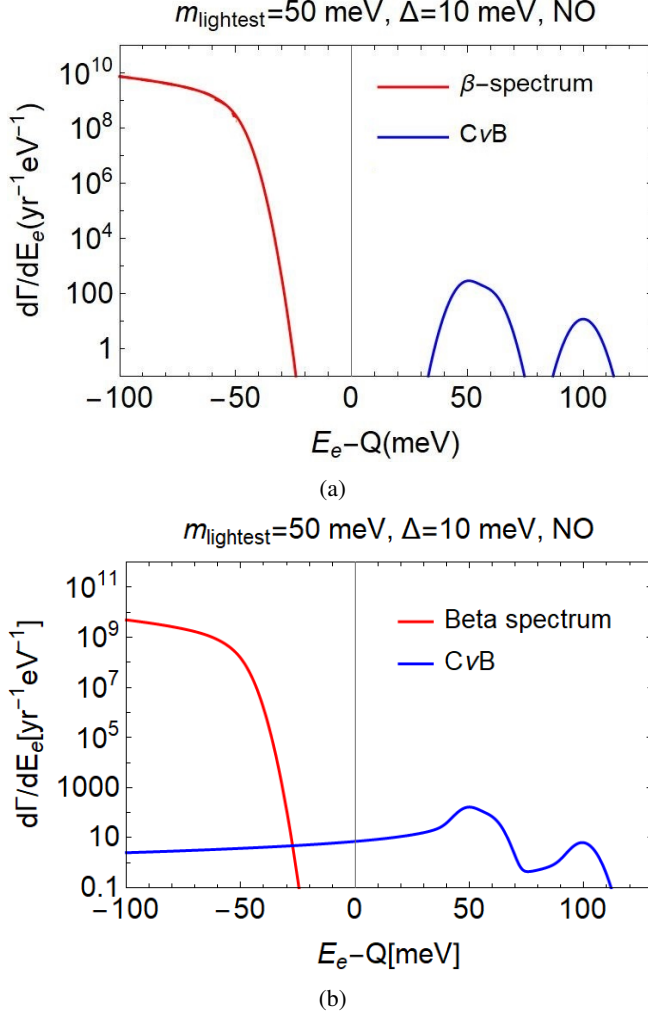


FIG. 6: Panel 6(a) shows the theoretical beta decay spectrum of mono-atomic tritium in vacuum assuming the lightest neutrino mass of 50 meV. The solid red curve represents the background beta decay. The solid blue curve represents the signal from the cosmic neutrino background. $d\Gamma/dE$ describes the possibility that the events happen at a given energy per year. The area under the curve represents the number of events per year. The area under the blue curve is only four, that is the calculation is done for the amount of Tritium that can capture at most four cosmic neutrinos per year. In the region where the beta decay background (red curve) overlaps with the $C\nu B$ (blue curve) one cannot distinguish the cosmic neutrino signal from noise. Panel 6(b) describes the beta decay spectrum adjusted for the Fermi sea shakeup effect. We choose the coupling constant $g = 0.125$.

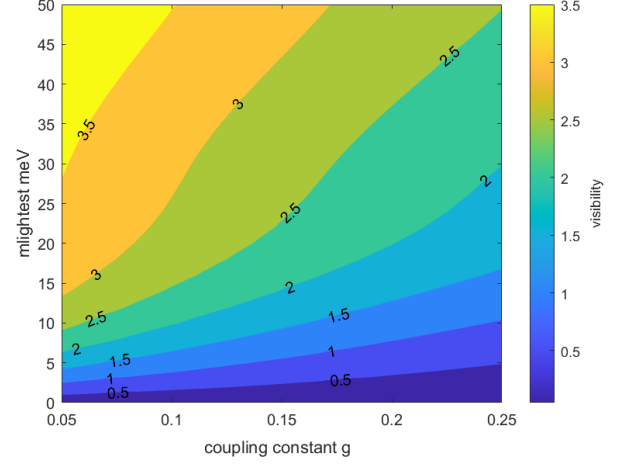


FIG. 7: Contour plot of visibility as a function of the lightest mass of neutrino and the coupling constant. The cut-off energy is assumed to be 1 eV. The maximum possible number of $C\nu B$ events is 4.

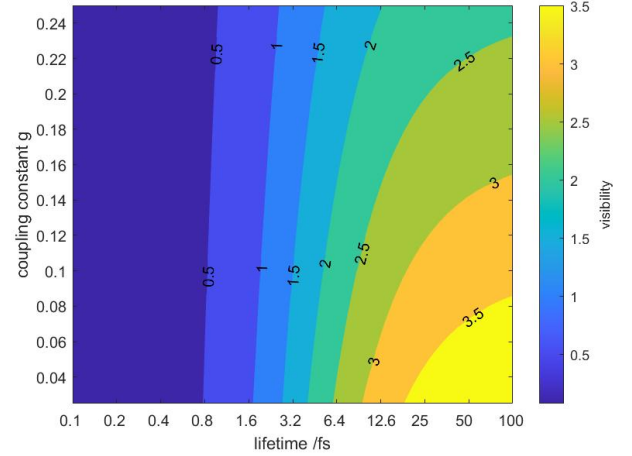


FIG. 8: Contour plot of visibility as a function of the coupling constant and the lifetime of the helium ion in fs.

SUMMARY AND OUTLOOK

In this work, we discussed how the shakeup of graphene's Fermi sea may influence the visibility of the cosmic neutrino signal in the PTOLEMY project. In the first section, we used Fermi's golden rule to find the beta decay spectrum adjusted for the Fermi sea shakeup effect. We found that it is the convolution between the spectral density function of graphene and the original beta decay spectrum function. Furthermore, we applied perturbation theory and the linked cluster expansion, to obtain the spectral density function, which is the Gamma distribution function and controlled by two parameters, the cutoff energy and the dimensionless coupling constant.

In the next section, we examined factors that influence

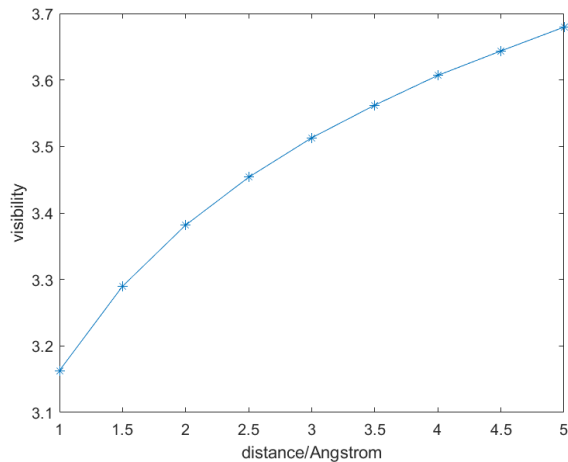


FIG. 9: Visibility at different heights with coupling constant $g = 0.1$, and $m_{\text{lightest}} = 50$ meV. The curves with different coupling constants and the neutrinos' lightest mass share a similar feature.

the coupling constant and the cutoff energy, and we also considered the influence of the Helium ion's lifetime on graphene's spectral density function. We found that the distance between the ion and graphene dictates the natural distance-dependent energy cutoff scale. Also, the disorder effects can be neglected if the concentration of the tritium atom is less than $5 \times 10^{11} \text{ cm}^{-2}$. However, the dynamic screening effects of the intrinsic graphene significantly increase the coupling constant, which is detrimental to the visibility of the PTOLEMY project. Fortunately, if the external dielectric constant of the substrate is large enough, the dynamic screening effects can be suppressed. We further established that the lifetime of the Helium ion may have a significant impact on the visibility of the PTOLEMY project if it is smaller than 1 fs. Overall, we have three main conclusions.

(1) Our preliminary analysis indicates that despite large energy scales associated with the shakeup of the Fermi sea, the visibility can still be protected by the X ray edge singularity and screening effects. Even though we refer to the radioactive atom as Tritium, our calculation is universal and all conclusions hold for other atoms.

(2) We suggest the following two ways to improve the visibility for the PTOLEMY project:

1) use a substrate with a high dielectric constant;

2) deposit the radioactive atoms in such a way as to maximize their distance from the graphene sheet.

(3) Not all effects are included in our analysis, so experiments should be conducted to test the validity range of our theory. The lifetime of the Helium ion cannot be calculated, so experiments should be conducted to measure it. We finally remark that although we have considered some important solid state effects that can affect the spectral density function, other effects require further study. Those include phonon emission,

inhomogeneous broadening in a disordered sample, Coulomb interaction of the beta-electron with electrons in graphene and others. While such effects are not necessarily important in the traditional X-ray emission experiment, the extraordinary energy resolution required by the PTOLEMY experiment puts unusually stringent constraints on the admissible rate and magnitude of disruption due to various solid state processes. We hope that further research will improve our understanding of such effects and their mitigation.

We wish to acknowledge Dr. Boyarksy to provide us the data. We also appreciate the discussion with Yevheniia Cheipesh. The first author especially wants to express his gratitude to his fiancée Yiping Deng for taking care of him when writing this paper.

* cheianov@lorentz.leidenuniv.nl

- [1] A. A. Penzias and R. W. Wilson, A Measurement of Excess Antenna Temperature at 4080 Mc/s., *Astrophysical Journal* **142**, 419 (1965).
- [2] C. L. Bennett, D. Larson, J. L. Weiland, N. Jarosik, G. Hinshaw, N. Odegard, K. Smith, R. Hill, B. Gold, M. Halpern, and others, Nine-year Wilkinson Microwave Anisotropy Probe (WMAP) observations: final maps and results, *The Astrophysical Journal Supplement Series* **208**, 20 (2013), publisher: IOP Publishing.
- [3] Planck Collaboration, *Planck* 2013 results. V. LFI calibration, *Astronomy & Astrophysics* **571**, A5 (2014).
- [4] S. Weinberg, Universal Neutrino Degeneracy, *Physical Review* **128**, 1457 (1962), publisher: American Physical Society.
- [5] Y. F. Li, Z.-z. Xing, and S. Luo, Direct detection of the cosmic neutrino background including light sterile neutrinos, *Physics Letters B* **692**, 261 (2010).
- [6] J. Angrik, T. Armbrust, and A. Beglarian, *KATRIN design report 2004*, Tech. Rep. (Forschungszentrum Karlsruhe GmbH Technik und Umwelt (Germany). Inst. fuer Kernphysik, 2005).
- [7] A. G. Cocco, G. Mangano, and M. Messina, Probing low energy neutrino backgrounds with neutrino capture on beta decaying nuclei, *Journal of Cosmology and Astroparticle Physics* **2007** (06), 015.
- [8] F. L. Wilson, Fermi's theory of beta decay, *American Journal of Physics* **36**, 1150 (1968), publisher: American Association of Physics Teachers.
- [9] We acknowledge Dr. Boyarksy to provide us the date and the Mathematica code.
- [10] L. I. Bodine, D. S. Parno, and R. G. H. Robertson, Assessment of molecular effects on neutrino mass measurements from tritium β decay, *Physical Review C* **91**, 035505 (2015).
- [11] S. Betts, W. Blanchard, R. Carnevale, C. Chang, C. Chen, S. Chidzik, L. Ciebiera, P. Cloessner, A. Cocco, A. Cohen, and others, Development of a relic neutrino detection experiment at PTOLEMY: princeton tritium observatory for light, early-universe, massive-neutrino yield, [arXiv preprint arXiv:1307.4738](https://arxiv.org/abs/1307.4738) (2013).
- [12] A. Faessler, R. Hodak, S. Kovalenko, and F. Šimkovic, Beta Decay and the Cosmic Neutrino Background, *EPJ Web of Conferences* **71**, 00044 (2014).
- [13] B. Monreal and J. A. Formaggio, Relativistic cyclotron radia-

- tion detection of tritium decay electrons as a new technique for measuring the neutrino mass, *Physical Review D* **80**, 051301 (2009).
- [14] S. Jonsell and H. J. Monkhorst, Effects from changes in the final state spectrum on the neutrino mass determination from t_2 beta decay experiments, *Physical review letters* **76**, 4476 (1996).
- [15] Z. Tan, *Effects of X ray edge in the Ptolemy project*, Master's thesis, Leiden University, the Netherlands (2021).
- [16] E. Baracchini, M. Betti, M. Biasotti, A. Bosca, F. Calle, J. Carabe-Lopez, G. Cavoto, C. Chang, A. Cocco, A. Colijn, and others, PTOLEMY: A proposal for thermal relic detection of massive neutrinos and directional detection of MeV dark matter, [arXiv preprint arXiv:1808.01892](https://arxiv.org/abs/1808.01892) (2018).
- [17] M. Betti, M. Biasotti, A. Bosca, F. Calle, N. Canci, G. Cavoto, C. Chang, A. Cocco, A. Colijn, J. Conrad, and others, Neutrino physics with the PTOLEMY project: active neutrino properties and the light sterile case, *Journal of Cosmology and Astroparticle Physics* **2019** (07), 047, publisher: IOP Publishing.
- [18] Y. V. Skrypnik and V. M. Loktev, Metal-insulator transition in hydrogenated graphene as manifestation of quasiparticle spectrum rearrangement of anomalous type, *Physical Review B* **83**, 085421 (2011), publisher: APS.
- [19] Y. Hochberg, Y. Kahn, M. Lisanti, C. G. Tully, and K. M. Zurek, Directional detection of dark matter with two-dimensional targets, *Physics Letters B* **772**, 239 (2017), publisher: Elsevier.
- [20] Y. Cheipesh, V. Cheianov, and A. Boyarsky, Heisenberg's uncertainty as a limiting factor for neutrino mass detection in β -decay, [arXiv preprint arXiv:2101.10069](https://arxiv.org/abs/2101.10069) (2021).
- [21] O. Mikulenko, Y. Cheipesh, V. Cheianov, and A. Boyarsky, Can we use heavy nuclei to detect relic neutrinos?, [arXiv preprint arXiv:2111.09292](https://arxiv.org/abs/2111.09292) (2021).
- [22] Y. Adamov and B. Muzykantskii, Fermi gas response to the nonadiabatic switching of an external potential, *Physical Review B* **64**, 245318 (2001).
- [23] G. D. Mahan, Excitons in Metals: Infinite Hole Mass, *Physical Review* **163**, 612 (1967).
- [24] B. Roulet, J. Gavoret, and P. Nozières, Singularities in the X-Ray Absorption and Emission of Metals. I. First-Order Parquet Calculation, *Physical Review* **178**, 1072 (1969).
- [25] P. Nozières, J. Gavoret, and B. Roulet, Singularities in the X-Ray Absorption and Emission of Metals. II. Self-Consistent Treatment of Divergences, *Physical Review* **178**, 1084 (1969).
- [26] P. NOzières and C. T. De Dominicis, Singularities in the X-Ray Absorption and Emission of Metals. III. One-Body Theory Exact Solution, *Physical Review* **178**, 1097 (1969).
- [27] K. D. Schotte and U. Schotte, Tomonaga's Model and the Threshold Singularity of X-Ray Spectra of Metals, *Physical Review* **182**, 479 (1969).
- [28] P. W. Anderson, Infrared Catastrophe in Fermi Gases with Local Scattering Potentials, *Physical Review Letters* **18**, 1049 (1967).
- [29] D. Chitwood, T. Banks, M. Barnes, S. Battu, R. Carey, S. Cheekatmalla, S. Clayton, J. Crnkovic, K. Crowe, P. Debevec, and others, Improved measurement of the positive-muon lifetime and determination of the Fermi constant, *Physical review letters* **99**, 032001 (2007), publisher: APS.
- [30] K. Ohtaka and Y. Tanabe, Theory of the soft-x-ray edge problem in simple metals: historical survey and recent developments, *Reviews of Modern Physics* **62**, 929 (1990).
- [31] M. Combescot and P. Nozières, Infrared catastrophe and excitons in the X-ray spectra of metals, *Journal de Physique* **32**, 913 (1971).
- [32] G. D. Mahan, *Many-Particle Physics* (Springer US, 2000) 3rd ed., pp. 90–94, 192–195, 325–335, 603–621.
- [33] G. Mahan, Many-body effects on x-ray spectra of metals, in *Solid State Physics*, Vol. 29 (Elsevier, 1974) pp. 75–138.
- [34] E. Kogan and M. Kaveh, On the X-Ray Edge Problem in Graphene, *Graphene* **7**, 1 (2018).
- [35] P. Brouwer, Theory of many particle system (unprinted, 2005) pp. 100–105.
- [36] E. H. Hwang and S. Das Sarma, Dielectric function, screening, and plasmons in two-dimensional graphene, *Physical Review B* **75**, 205418 (2007).
- [37] M. I. Katsnelson, *The Physics of Graphene* (Cambridge University Press, 2020) 2nd ed., pp. 141–145, 181–186.
- [38] K. W. K. Shung, Dielectric function and plasmon structure of stage-1 intercalated graphite, *Physical Review B* **34**, 979 (1986).
- [39] G. Giuliani and G. Vignale, *Quantum theory of the electron liquid* (Cambridge university press, 2005) pp. 160–170, 177–181.
- [40] N. D. Mermin, Lindhard Dielectric Function in the Relaxation-Time Approximation, *Physical Review B* **1**, 2362 (1970).
- [41] F. Giannazzo, S. Sonde, R. L. Nigro, E. Rimini, and V. Raineri, Mapping the density of scattering centers limiting the electron mean free path in graphene, *Nano letters* **11**, 4612 (2011), publisher: ACS Publications.
- [42] L. Banszerus, M. Schmitz, S. Engels, M. Goldsche, K. Watanabe, T. Taniguchi, B. Beschoten, and C. Stampfer, Ballistic transport exceeding $28 \mu\text{m}$ in CVD grown graphene, *Nano letters* **16**, 1387 (2016), publisher: ACS Publications.
- [43] M. Bonfanti, S. Achilli, and R. Martinazzo, Sticking of atomic hydrogen on graphene, *Journal of Physics: Condensed Matter* **30**, 283002 (2018).
- [44] H. González-Herrero, E. Cortés-del Río, P. Mallet, J. Veuillen, J. Palacios, J. Gómez-Rodríguez, I. Brihuega, and F. Ynduráin, Hydrogen physisorption channel on graphene: a highway for atomic H diffusion, *2D Materials* **6**, 021004 (2019), publisher: IOP Publishing.
- [45] M. Moaied, J. A. Moreno, M. J. Caturla, F. Ynduráin, and J. J. Palacios, A theoretical study of the dynamics of atomic hydrogen on graphene bilayers, *Physical Review B* **91**, 155419 (2015), [arXiv: 1405.3165](https://arxiv.org/abs/1405.3165).
- [46] F. Ding and B. I. Yakobson, Challenges in hydrogen adsorptions: from physisorption to chemisorption, *Frontiers of Physics* **6**, 142 (2011).
- [47] T. Stauber, N. M. R. Peres, and F. Guinea, Electronic transport in graphene: A semiclassical approach including midgap states, *Physical Review B* **76**, 205423 (2007).
- [48] M. Hentschel and F. Guinea, Orthogonality catastrophe and Kondo effect in graphene, *Physical Review B* **76**, 115407 (2007).
- [49] G. Canright, Time-dependent screening in the electron gas, *Physical Review B* **38**, 1647 (1988), publisher: APS.

APPENDIX

A1

The details of obtaining the natural cutoff energy are presented here.

Substituting eq. (34) into the eq. (22), one can find that

$$F_2'(t) = -g \int_0^{\xi_0} \frac{(1 - e^{-iut}) du}{u} - \frac{\pi g}{2} \int_0^{\xi_0} du \frac{(1 - e^{-iut})}{u} \left[L_1\left(\frac{2du}{v_F}\right) - I_1\left(\frac{2du}{v_F}\right) \right] \quad (57)$$

The first integration is the original term, labeled as $F_2^0(t)$ and the second integration is the correction term, labeled as $F_2'(t)$. Directly evaluating the correction term is difficult, but we can express it as a double integral.

$$F_2'(t) = g \int_0^{2d\xi_0/v_F} \int_0^1 e^{-zx} \sqrt{1-x^2} (1 - e^{-izv_F t/2d}) dx dz = P(\xi_0) + N(\xi_0, t) \quad (58)$$

where

$$P(\xi_0) = g \int_0^1 dx \sqrt{1-x^2} \left(\frac{1 - e^{-2dx\xi_0/v_F}}{x} \right), \quad (59)$$

and

$$N(\xi_0, t) = g \int_0^1 dx \sqrt{1-x^2} \left(\frac{-1 + \exp(-it\xi_0 - 2dx\xi_0/v_F)}{x + iv_F t/2d} \right) \quad (60)$$

with $z = 2du/v_F$. From the calculation above, we can find that the correction term can be split into two terms. The first part is a constant independent of time t , and the second part is a time-dependent function. Hence, only the function $N(\xi_0, t)$ is significant to our calculation. Obviously, if $t = 0$, it cancels with the first term $P(\xi_0)$. However, when t approaches infinity, the correction term $F_2'(t)$ should equal to $P(\xi_0)$. We need to make some approximations to evaluate the function $N(\xi_0, t)$.

At a large time limit, roughly, we can use 1 to replace the ugly square root $\sqrt{1-x^2}$ since most contributions to the integration in $P(\xi_0)$ and $N(\xi_0, t)$ come from the vicinity of $x=0$. Then, we can write the correction term $F_2'(t)$ in a simple way.

$$\begin{aligned} F_2'(t) &= g \int_0^1 \left(\frac{1 - e^{-2dx\xi_0/v_F}}{x} \right) dx \\ &\quad + g \int_0^1 dx \left(\frac{-1 + \exp(-it\xi_0 - 2dx\xi_0/v_F)}{x + iv_F t/2d} \right) \\ &= g \int_0^1 \left(\frac{1 - e^{-2dx\xi_0/v_F}}{x} \right) dx \\ &\quad - g \int_{iv_F t/2d}^{1+iv_F t/2d} \left(\frac{1 - \exp(-2dy\xi_0/v_F)}{y} \right) dy \\ &= g \int_0^1 \left(\frac{1 - e^{-2dx\xi_0/v_F}}{x} \right) dx \\ &\quad + g \int_0^{iv_F t/2d} \left(\frac{1 - \exp(-2dy\xi_0/v_F)}{y} \right) dy \\ &\quad - g \int_0^{1+iv_F t/2d} \left(\frac{1 - \exp(-2dy\xi_0/v_F)}{y} \right) dy \end{aligned} \quad (61)$$

The factor $1 - \exp(-2dy\xi_0/v_F)$ behaves as $2dy\xi_0/v_F$ in the limit $u \rightarrow 0$. We can use $\frac{v_F}{2d\xi_0}$ to replace the lower limit of the integration, since $\frac{v_F}{2d\xi_0} \ll 1$. At very large time t , we omit the factor $\exp(-2dy\xi_0/v_F)$. Hence, the correction term $F_2'(t)$ can be approximately expressed as a very neat form.

$$\begin{aligned} F_2'(t) &\approx g \int_{v_F/(2d\xi_0)}^1 \frac{dx}{x} + g \int_{v_F/(2d\xi_0)}^{iv_F t/2d} \frac{dy}{y} \\ &\quad - g \int_{v_F/(2d\xi_0)}^{1+iv_F t/2d} \frac{dy}{y} \\ &\approx g \ln\left(1 + \frac{2d\xi_0}{v_F}\right) + g \ln(i\xi_0 t + 1) \\ &\quad - g \ln(i\xi_0 t + \frac{2d\xi_0}{v_F} + 1) \end{aligned} \quad (62)$$

Substituting eq. (62) into equation (57), and using equation (20) and equation (32), one can obtain the expression of spectral density function of graphene.

$$\begin{aligned} A(\Omega') &= \int_{-\infty}^{\infty} \frac{dt}{2\pi} e^{-iEt} \exp(F_2^0(t) + F_2'(t)) \\ &= \Theta(-\Omega') \frac{\exp(\Omega')}{\Gamma(g)\xi'(-\Omega')^{(1-g)}} \end{aligned} \quad (63)$$

where $\xi' = \frac{\xi_0}{1+2d\xi_0/v_F}$, and $\Omega' = (E + E_i)/\xi'$.

The cut-off energy ξ_0 is entirely arbitrary, but we can get a natural cut-off energy ξ when we extend ξ_0 to infinity.

$$\xi = \lim_{\xi_0 \rightarrow \infty} \frac{\xi_0}{1 + 2d\xi_0/v_F} = \frac{\hbar v_F}{2d} \quad (64)$$

We get nearly the same result as the previous one, eq. (32), only with different cutoff energy ξ .

A2

For intrinsic graphene, the time-dependent potential is

$$V(q, t) = \frac{V(q)\theta(t)}{\epsilon(q, 0)} + V(q)\theta(t)T(v_F qt). \quad (65)$$

$T(v_F qt)$ is a one-variable fast-decay function that only depends $v_F qt$.

$$T(v_F qt) = -\frac{2}{\pi} \int_1^{\infty} \frac{a \cos(\omega v_F qt) \sqrt{\omega^2 - 1}}{\omega (\omega^2 - 1 + a^2)} d\omega, \quad (66)$$

where $a = (\epsilon(q, 0) - 1) = \frac{\pi e^2}{2\hbar\kappa v_F}$. When $t \ll 1$, $T(v_F qt) \approx \frac{1}{\epsilon(q, 0)} - 1$, and when $t \gg 1$, $T(v_F qt) \approx 0$. From the general expression of the $F_2(t)$, eq. (22), we can

find that

$$F_2(t) = \frac{1}{2} \int_0^t dt_1 \int_0^t dt_2 \int_0^\infty e^{-iu(t_1-t_2)} \frac{du}{\pi V} \\ \times \sum_q \left[\frac{1}{\epsilon^2(q, 0)} + \frac{T(v_F q t_1)}{\epsilon(q, 0)} + \frac{T(v_F q t_2)}{\epsilon(q, 0)} + \right. \\ \left. T(v_F q t_1) T(v_F q t_2) \right] |V(q)|^2 \Lambda(q, u) \quad (67)$$

When $t \ll 1$, then we can find $F_2(t) \approx 0$. It is trivial and has no contribution to the spectral density function. Therefore, the most significant part of the X-ray edge is in the long-time domain, and the function $T(v_F q t)$ decays very fast, so $T(v_F q t_1) T(v_F q t_2)$ is negligible compared to other terms in

the bracket. Therefore, one can get

$$F_2(t) \approx F_2^0(t) - \frac{gu\epsilon}{2} \int_0^t dt_1 \int_0^t dt_2 \int_0^\infty e^{-iu(t_1-t_2)} du \\ \times \int_1^\infty \frac{aH_{-1}(u\omega t_1) \sqrt{\omega^2 - 1}}{\omega(\omega^2 - 1 + a^2)} d\omega \\ - \frac{gu\epsilon}{2} \int_0^t dt_1 \int_0^t dt_2 \int_0^\infty e^{-iu(t_1-t_2)} du \\ \times \int_1^\infty \frac{aH_{-1}(u\omega t_2) \sqrt{\omega^2 - 1}}{\omega(\omega^2 - 1 + a^2)} d\omega, \quad (68)$$

where $F_2^0(t)$ is the original term in eq.(22) without considering dynamic screen effect. In the long time limit, we can extend t into infinity, and then one can get

$$F_2(t) \approx F_2^0(t) + \int_{i/t}^{\xi_0} \frac{2g\epsilon}{\pi u} du \int_1^\infty \frac{a \log(\omega + \sqrt{\omega^2 - 1})}{\omega^2(\omega^2 - 1 + a^2)} d\omega \\ \approx \log(1 + g_1 i \xi_0 t) \quad (69)$$

with

$$g_1 = g + \int_1^\infty \frac{2g\epsilon a \log(\omega + \sqrt{\omega^2 - 1})}{\pi \omega^2(\omega^2 - 1 + a^2)} d\omega \quad (70)$$

Therefore, the spectral density function has the same form as the previous result in eq. (32), but with a different coupling constant.